AGARD-CP-80-71
AGARD Conference Proceedings No.80

NORTH ATLANTIC TREATY ORGANIZATION

ADVISORY GROUP FOR AEROSPACE RESEARCH AND DEVELOPMENT

(ORGANISATION DU TRAITE DE L'ATLANTIQUE NORD)

SYMPOSIUM ON
UNSTEADY AERODYNAMICS FOR AEROELASTIC ANALYSES OF INTERFERING SURFACES

Published in Two Parts

PART II

Symposium on Unsteady Aerodynamics, Agard Structures and Materials Panel, Tønsberg, Norway, 3-4 Nov 1970.

Papers presented at the Symposium on Unsteady Aerodynamics, in conjunction with the 31st Meeting of the Structures and Materials Panel of AGARD, 3 and 4 November 1970, Tønsberg, Norway.

Part of the material in this publication has been reproduced directly from copy supplied by AGARD.

Published April 1971

L.C.71-155457
U.D.C.061.3:533.6.013.42:533.695

Printed by Technical Editing and Reproduction Ltd
Harford House, 7-9 Charlotte St, London. W1P 1HD

FOREWORD

A Symposium on Unsteady Aerodynamics for Aeroelastic Analyses of Interfering Surfaces was organized by the Structures and Materials Panel of AGARD in conjunction with its 31st meeting in Tønsberg, Norway, in November 1970. It was attended by approximately 60 participants from ten nations. The papers given on this occasion have been collected in the two volumes which I have the honour of presenting to the scientific audience of NATO.

One of the major concerns of the Structures and Materials Panel is the development of analytical and practical methods for predicting, preventing and controlling aeroelastic problems affecting both aircraft and aerospace-craft. Whether flutter, gust response, or alleviation and mode stabilization system designs are concerned, the development of safe and efficient methods depends on the ability to predict unsteady aerodynamic forces accurately.

As early as 1964, a Working Group created within The Structures and Materials Panel for the purpose of studying these forces, defined a small number of wing planforms to be used as standard models for comparing aerodynamic force prediction methods on the basis of data on vibration modes, excitation frequencies and Mach numbers. In view of the tremendous utility of such a scheme, the Panel decided in 1968 to extend this programme to include the interaction of more complex aerofoils such as T-tails or wing horizontal tail combinations. Several planforms, as well as some parameters, have been recently selected to be used as standards for comparisons.

Consequently, the objectives and themes of the Symposium have been set as follows:

(a) Present and discuss the latest contributions to methods for predicting unsteady aerodynamic forces in the interactions of lifting surfaces.

(b) Determine the merits and limitations of various methods.

(c) Present applications and numerical values which can be employed to evaluate the new methods proposed.

(d) Formulate suggestions about future developments and requirements.

The papers presented have been arranged in five sections:

I. Methods using the lifting surface equation.

II. Methods using a lattice or lifting lines.

III. Application to the calculation of unsteady interaction forces.

IV. Testing and application to flutter.

V. Wing-control surface interactions.

In view of their general scope, four of these papers have been selected by the Panel as contributions to the Manual on Aeroelasticity (in six volumes), published by AGARD on the initiative of the Panel. These four papers, the titles of which are listed below, have been collected in Part I of the Conference Proceedings in order to be included in the Manual:

– H.ASHLEY	"Some Considerations Relative to the Prediction of Unsteady Airloads of Interfering Surfaces (Introductory Paper)" – to be included in Volume II, Chapter 1.
– D.E.DAVIES	"Calculation Methods for Unsteady Airforces on Tandem Surfaces and T-tails in Subsonic Flow" – to be included in Volume II, Chapter 3.
– R.DAT and Y.AKAMATSU	"Representation of a Wing by Lifting Lines. Application to the Calculation of the Interaction of Two Wings in Tandem" – to be included in Volume II, Chapter 3.
– D.L.WOODCOCK and E.YORK	"A Supersonic Box Collocation Method for the Calculation of Unsteady Airforces on Tandem Surfaces" – to be included in Volume II, Chapter 5.

The other eleven papers have been collected in Part II of the Conference Proceedings. While these are also of great interest, either they have already been published elsewhere for their major part, or the discussions which followed them revealed some divergences of an experimental nature bringing out the existence of many yet unsolved problems. Surely the usefulness and value of such a meeting lies precisely in this: to provide specialists of entirely different origins and training with the opportunity of discussing together a fundamental problem in constant development and, thus, of evaluating the progress made so far and that still to be accomplished.

R.MAZET
Programme Committee Chairman

SYMPOSIUM CHAIRMAN

Professor R.MAZET
Professor à la Faculté des
Sciences de Paris
91-Orsay, France

SYMPOSIUM VICE-CHAIRMAN

Prof. Dr Ing.H.G.KÜSSNER
Aerodynamische Versuchsanstalt Göttingen e.V.
34-Göttingen
Germany

PROGRAMME COMMITTEE

Dr Ing.B.LASCHKA
VFW-Fokker GmbH und
Deutsche Airbus GmbH
8-Munchen, Germany

Mr.W.J.MYKYTOW
Assistant for Research
and Development
AF Flight Dynamics Laboratory
Wright-Patterson AFB, Ohio 45433
USA

PANEL EXECUTIVE

Peter K.BAMBERG
AGARD

CONTENTS

Papers annotated with an asterisk (*) are contained in PART I, those without, in PART II.

APPLICATION OF AFFDL UNSTEADY LOAD PREDICTION METHODS TO INTERFERING SURFACES

W.J.Mykytow, J.J.Olsen and S.J.Pollock

1. INTRODUCTION

An integral equation for subsonic flow, relating the non-dimensional downwash distribution to the product of pressure distribution and a kernel function, was formulated by Kussner[1] in 1940. This basic contribution provided a firm foundation for developments in the years to follow. However, many years elapsed before Watkins, Runyan, and Woolston[2] developed practical solutions and applications using numerical methods. Developments in the USA from about 1950 to 1964, were largely spent in applying methods developed by Watkins and his co-workers[3]. It can be said that because of these developments in the kernel function method and also the doublet-lattice method (to be discussed later), there has occurred in recent years a remarkable increase in the ability to predict with accuracy the forces on isolated, stationary or oscillating lifting surfaces in subsonic flow. Particularly notable among recent improvements of subsonic methods is the work on planar wings by Rowe[4], Cunningham[5], and Albano and Rodden[6] and the work on control surfaces by Berman[7], Landahl[8], and Ashley and Rowe[9].

With regard to interference effects, in the 1960's, Ashley[10,11,12] extended the earlier ideas of subsonic and supersonic lifting surface theory to the development of the subsonic kernel function and supersonic velocity potential influence coefficient methods to nonplanar surfaces. Using those ideas, several methods have been developed under AFFDL auspices. Some have been more successful than others in meeting their goals, but all can be said to have extended the state-of-the-art in some respect. References 7, and 13–24 are some of the reports presented over the last several years, first applying the original lifting surface methods to planar wings, and then extending them to cases of mutual interference. Workable methods which incorporate the effects of interference between different surfaces have long been needed for T-tails – a requirement not quite yet completely satisfied. They have also proved to be invaluable in understanding the flutter of wing-tail combinations, important aspects of which cannot be evaluated by isolated surface aerodynamics.

The purpose of the effort described herein is to apply newly developed methods in an engineering fashion, to evaluate them and to determine their merits and limits. This paper thus presents some of the recent results obtained with computer programs developed for:

1. Subsonic flow over wing-tail combinations (FDL-TDR-70-59, Reference 23).
2. Supersonic flow over wings with folded tips, T-tails and cruciform tails (FDL-TDR-64-152, Part VI, Reference 19).

2. BRIEF DISCUSSION OF THE METHODS

2.1 The Subsonic Kernel Function Program for Wing-Tail Configurations

The kernel function program for wing-tail configurations has been developed by Albano[23] and is an implementation and extension of the method of Laschka[26,27,28]. The usual integral equation is used to solve for the lift distribution $l(\xi,\eta)$ given the prescribed downwash $w(x,y,z)$:

$$w(x,y,z) = \iint K(x,y,z;\xi,\eta,\zeta)\, l(\xi,\eta,\zeta)\, \frac{dS}{s^2} \ .$$

Landahl's[29] improvement of the Rodemich[16] kernel function is used, together with an expansion due to Watkins[2] in the evaluation of integrals familiarly known as I_1 and I_2. The lift distribution is taken for wing and tail in the form of prescribed functions $h_i(x)$ and unknown coefficients $a_i(y)$:

$$l(x,y) = \sum_{i=1}^{N} a_i(y) h_i(x) \frac{s}{c(y)} \ .$$

Following Laschka, the terms in the kernel function which are singular when $\eta \to y$ are separated from the part with regular behavior, leading to three types of improper chordwise integrals I_{1i}, I_{2i}, and I_{3i} so that the equation for the downwash becomes

$$w(x,y) = \sum_{i=1}^{N} \int_{-1}^{1} a_i(\eta) \left\{ \frac{I_{1i}}{(y-\eta)^2} + ihI_{2i} + \frac{h^2}{2} I_{2i} + \int_0^1 (K - K_s) h_i(\xi) d\xi \right\} d\eta \, .$$

This equation is then converted to one involving a spanwise integration involving functions f_{1i}, f_{2i}, f_{3i} which are themselves bounded and continuous and which are evaluated using Laschka's techniques. The result is

$$w(x,y) = \sum_{i=1}^{N} \left\{ \int_{-1}^{1} \frac{a_i f_{1i}}{(y-\eta)^2} d\eta - \int_{-1}^{1} a_i \log_e |y-\eta| f_{2i} d\eta + \int_{-1}^{1} a_i f_{3i} d\eta \right\}.$$

At this point, a sine series is assumed for the products $a_i f_{ki}$ and numerical integrations are carried out by Multhopp's, Laschka's, and Gaussian quadratures, respectively. Following the spanwise integration, collocation is used to evaluate the unknown coefficients a_i using Multhopp's spanwise stations and chordwise collocation stations which Stark[30] has shown to be optimum. Advantage is taken of the fact that some of the singularities are not present in evaluating the effect of the tail on the wing and that still more are absent when the two surfaces lie in different planes.

The final computer program may be used for: (a) coplanar wing-tail, (b) wing and tail in different, but parallel, planes, and (c) wing and tail in different planes with tail dihedral. Applications (b) and (c) require a vertical separation of at least 10–15% semispan.

2.2 The Doublet-Lattice Method for Wing-Tail Configurations and Intersecting Surfaces

The doublet-lattice method for wing-tail configurations and intersecting surfaces is based on developments by Albano and Rodden[6]. The surfaces are divided into trapezoidal panels, the downwash being taken at the 3/4 chord, midspan of each panel. The 1/4 chord of each panel contains a distribution of acceleration potential doublets whose strength is to be determined. The force on the panel due to the lift distribution is assumed to equal the force on the doublet line segment. The inner details require integrals of the kernel function along line segments. In the initial program the integrals were obtained by approximating the kernel in each box with a parabola in the spanwise direction divided by r_1^2, where $r_1^2 = y_0^2 + z_0^2$ and where y_0, z_0 are relative y and z distances. Considering the simplifying assumptions made, the accuracy of this method has been remarkable. For day-to-day applications, the versatility and ease of application have proved to be of substantial benefit.

A second generation doublet-lattice method has been developed by Kalman, Rodden, and Giesing[31] for applications to more general configurations, and many applications have been made to isolated wings, wings with controls, wing-tail interference, and intersecting surfaces. They[25] are now extending the method to include wing-body interference and are developing a computer program for the AFFDL. In the process of extending methods to include wing-body interference, Rodden appears to have removed the previously mentioned difficulty for small vertical separation between two surfaces. He observed that terms in the non-planar kernel function varied like r^{-4} rather than r^{-2} for the planar terms. Use of a parabola was retained to represent variation of the numerator with span along a box 1/4 chord line, but an r_1^4 variation was used in the denominator. This resulted in a smooth variation of force coefficients with decreasing vertical separation of two surfaces. The final development of the method will employ the doublet-lattice procedure for lifting surfaces with an image system in the body, a steady axial source distribution for fuselage and store volume effects, and an unsteady axial doublet distribution for angle of attack and camber effects. At the time of this writing, the second generation program was not yet completely checked out on the AFFDL computer.

2.3 The Mach Box Method for General Arrays of Intersecting Surfaces

The Mach box method for general arrays of intersecting planar surfaces is an extension by Andrew[19] of the work of Andrew and Moore[18]. When complete, the associated computer program should be able to determine unsteady generalized forces for many configurations with intersecting surfaces. All physical and "diaphragm" surfaces are subdivided into identical "Mach boxes", and the downwash is taken at the center of each box. The source strength to be determined is assumed to be constant in each box, except in the two rows of boxes immediately adjacent to a line of surface intersection. In the two rows adjacent to a line of intersection, the usual source strength is augmented by an additional strength term which behaves like $\lambda/(y - y_F)$, where λ is to be determined. An area correction is used to estimate source strengths of boxes cut by a leading edge, and the method of least squares is used to fit a polynomial to the velocity potential so as to provide correct behavior near edges.

3. APPLICATIONS

3.1 The Kernel Function and Doublet-Lattice Methods for Wing-Tail Configurations

The configurations used for application of these two methods are shown in Figure 1. They are: the wing-tail combination proposed by AGARD as a standard for comparison, the configuration analyzed by Laschka and Schmid[27], the flutter model tested by Cornell Aeronautical Laboratory at transonic speeds[32], and the model tested by the Air Force Flight Dynamics Laboratory at subsonic speeds[33]. The methods to be applied to the various configurations are:

(a) AGARD Configuration
  (i) Isolated Surfaces (Kernel Function and Doublet-Lattice)
  (ii) Coplanar Surfaces (Kernel Function and Doublet-Lattice)
  (iii) Vertical Separation (Kernel Function)
  (iv) Dihedral with Vertical Separation (Kernel Function)
  (v) A Biplane Configuration (Kernel Function)

(b) AFFDL Flutter Model (Kernel Function and Doublet-Lattice)

(c) Cornell Flutter Model (Kernel Function and Doublet-Lattice)

(d) Laschka-Schmid Configuration (Kernel Function and Doublet-Lattice).

(a) *The AGARD Configuration*

In all cases, the mode shapes are antisymmetric and in AGARD notation:

Wing

$$f_1 = y(x - 2.25|y| - 0.85)$$

$$f_2 = y|y| .$$

Horizontal Tail

$$f_3 = y$$

$$f_4 = (x - 3.35)(\text{Sign of } y) ,$$

where all dimensions and displacements are referred to the wing semispan, s .

Isolated Surfaces

The comparison of the results of the subsonic kernel function and the subsonic doublet-lattice method is first shown for the case when the wing or tail is isolated, and there is no interference. The doublet-lattice method was applied with the semi-span of the wing broken into two sections. The inboard section had 4 spanwise and 10 chordwise boxes; the outboard section had 5 spanwise and 8 chordwise boxes. The tail was similarly broken into two sections – a 4 x 7 array inboard and a 5 x 4 array outboard. The kernel function method was applied with 15 spanwise and 4 chordwise collocation points for each surface. Table I gives the AGARD generalized force coefficients Q'_{ij} and Q''_{ij} for $k = s\omega/V = 0.01$ and 1.5 and at $M_\infty = 0.8$, where

$$Q_{ij} = \frac{-1}{2q}\int_{-1}^{1}\int_{x_L}^{x_T} f_i \Delta p_j \, dx\, dy = Q'_{ij} + i(s\omega/V)Q''_{ij} .$$

Almost all coefficients agree within 10%. A few of the real coefficients show discrepancy. However, when the total coefficient is considered as a vector, the agreement in modulus and phase is quite good. Generally speaking, the agreement is within the variation each method would produce by a different box array or selection of collocation points.

Coplanar Surfaces

For application to the interfering coplanar surfaces, the doublet-lattice method was employed with an array of 8 semispan x 6 chordwise boxes on the wing and an array of 8 semispan x 4 chordwise boxes on the tail. The kernel function method was again used with 15 spanwise and 4 chordwise collocation points. Tables II and III give the comparison of AGARD generalized force coefficients for $s\omega/V = 0.01$ and 1.5 for $M_\infty = 0.8$. The tabulated results show fairly good agreement. Some differences are noticeable; the generalized forces in tail pitch due to tail pitch and wing twist due to wing twist both show differences exceeding 10%. More detailed information about the differences is contained in the chordwise pressure distributions due to wing twist given in Figure 2. These results are for $M_\infty = 0.8$, $s\omega/V = 1.5$, and a station located at 56% semispan, and are augmented by a similar comparison of section lift coefficients in Figure 3 and section moment coefficients in Figure 4. The pressures from the doublet-lattice program are plotted at the box 1/4 chords. The moment coefficients are approximate in that the pressure is

assumed to act at the 1/4 chord of each box. The pressure distributions at 56% semispan due to wing twist in Figure 2 show a reassuring amount of similarity between the two methods. Although the pressure distributions are roughly the same, the kernel function method systematically seems to produce larger pressure peaks at this mid-semispan position. Examination of the section lift and moment coefficients of Figures 3 and 4 shows again that the kernel function method usually gives higher peak values, particularly at inboard stations. The maximum section lifts and moments for the doublet-lattice are shifted slightly outboard. The largest disagreement between the kernel function and doublet-lattice results appears in the imaginary part of the pressure, lift, and moment on the tail due to wing twist. This may be due in large measure to the limited number of boxes which were available in the initial doublet-lattice program. Since 8 semispan boxes were used to adequately represent spanwise variations of downwash and pressure, the number of chordwise boxes on the tail was limited to 4. The second generation program removes that restriction so that the number of chordwise boxes on the tail can be increased for later calculations.

For the sake of brevity, only a few results for all the calculations conducted have been given here, and some variations are to be expected within each method for different locations of collocation points, numbers of boxes, etc. However, our calculations over a wide range of variables are represented reasonably well by the above data.

Vertical Separation

As mentioned earlier, the initial version of the doublet-lattice method could be used only for coplanar wing-tail configurations, and the improvements by Giesing, Kalman and Rodden[25,31] were not yet available for the calculations of this paper. Therefore, this subsection presents only kernel function results for the case where there is vertical separation between wing and horizontal tail, and the tail has dihedral. Again, using the AGARD wing-tail configuration, the horizontal tail was raised to a distance of 0.6 semispan above the plane of the wing. Tables IV and V illustrate the change in the generalized force coefficients obtained with the same array of 15 x 4 collocation points. Figure 5 shows the lift and moment coefficients on the wing and tail due to wing twist at $s\omega/V = 0.01$. The position of the tail has little effect on the wing, but produces significant reductions of the tail lifts and moments due to wing motions when the tail is raised.

Dihedral Effects with Vertical Separation

With the tail elevated to $\Delta z = 0.6$ above the plane of the wing, kernel function calculations were performed for a tail dihedral of $\pm 30^\circ$ with 15 x 4 collocation points at $M_\infty = 0.8$ and $s\omega/V = 0.01$ and 1.5. Tables VI and VII give the resulting generalized force coefficients compared to the coefficients for zero dihedral. Those coefficients which represent pressure on the wing due to wing motion and pressures on the tail due to tail motion are nearly constant, as anticipated. The largest effect is in the forces on the tail due to wing motion, and negative dihedral has a much larger effect than positive dihedral since the tail is brought closer to the wing. These trends are illustrated further in Figure 6 where the wing and tail C_l and C_m due to wing twist are shown for $s\omega/V = 0.01$. The effects of negative dihedral can be compared with those of positive dihedral.

A Biplane Configuration

The AGARD wing was also used as two planforms with one planform directly above the other. The kernel function method was applied to this biplane with one surface pitching and the other surface fixed for $s\omega/V = 1.0$ at $M_\infty = 0.8$. Figure 7 gives the real part of the section lift on each surface due to pitch of one of them. Results are given for vertical separations of 30, 50 and 100% of the semispan and show the increase in overall lift as the two surfaces move closer together.

(b) *The AFFDL Flutter Model*

The initial doublet-lattice program was also applied to a half-span flutter model which was tested by the AFFDL[33] at low subsonic velocities. This flutter model roughly represented a fighter and incorporated a variable sweep wing, variable fuselage torsional frequency and variable longitudinal spacing. The wing-pivot assembly had typical pitch and roll stiffnesses scaled to represent possible airplane values. One configuration of the horizontal tail permitted rotating the tail plane so as to give a 45 degree dihedral angle between the wing and tail planes. Some of the typical test results are shown in Figure 8 for 60 degrees of wing sweep along with the results calculated from the doublet-lattice method. It can be seen that the agreement is good, particularly when it is realized that the comparison is being made for the most sensitive or lowest velocity region. Also, viscous and wing thickness effects probably caused less than ideal flow over the stabilizer and contributed to discrepancies between calculated and test results. The coplanar predictions are 15–20% conservative for critical frequency ratios, and agreement improves significantly with higher frequency ratios. The kernel function method was used to check the coplanar doublet-lattice results and gave identical results. The maximum reduced frequency ($s\omega/V$) for the flutter model cases was about 0.05. Δx is the model horizontal wing-tail separation.

Also, although the present kernel function method could not be used to evaluate dihedral effects in the absence of vertical separation, it did predict the same trends as the dihedral was varied in the calculations with a given vertical displacement, $\Delta z = 20\%$ span. The second generation doublet-lattice program will be used at a later date to predict the effects of dihedral and to compare results against experimental data.

(c) *The Cornell Flutter Model*

The Cornell Aeronautical Laboratory constructed and tested some constant chord wing-horizontal tail flutter models[32] for the AFFDL. Wing and tail planforms were identical, and sweep angles for both surfaces were either 45 or 60 degrees. The torsional frequency of the mechanism connecting the two planforms could be varied. Figure 9 gives typical experimental data obtained for high subsonic and transonic speeds. The velocity has been non-dimensionalized by dividing by semi-chord times torsional frequency times square root of the wing to air density ratio. Figure 9 shows data for a vertical separation of 0.4 times semi-chord and a horizontal separation of one semi-chord. Albano's[23] applications of the kernel function method are shown, and these predicted results agree very well with the corresponding experimental data. Satisfactory agreement between experimental and analytical results was found for a wide range of vertical and longitudinal tail positions as is indicated by other results shown in Figure 9. All symbols are experimental data while all lines indicate predicted trends.

(d) *The Laschka-Schmid Configuration*

Both the kernel function and the doublet-lattice methods were used for calculations for the Laschka-Schmid configuration[27] of Figure 1. The kernel function used 15 x 3 collocation points. The doublet-lattice used an array of 9 semispan by 5 chordwise boxes on the wing and 6 semispan by 5 chordwise boxes on the tail. The modes used were: wing plunge, wing pitch, tail plunge, tail pitch. Figure 10 gives plots of the generalized force coefficients in Laschka's notation versus M_∞ for $s\omega/V = 1.0$ for wing or tail pitching modes. The generalized force coefficients are: lift and moment coefficients C_A and C_m respectively. Subscripts 11, 12, 21 and 22 denote force or moment on the wing due to wing pitch, on the wing due to tail pitch, on the tail due to wing pitch and on the tail due to tail pitch. The agreement among Laschka's kernel function results, Albano's implementation of the kernel function method using Laschka's approaches, and the doublet-lattice program is excellent.

In an unpublished note, J.Berman of Grumman Aerospace has given results for this configuration using a doublet-lattice program obtained from Stark of SAAB. The agreement with the results of the various methods mentioned above is generally good and is consistent with the results shown in Figure 10. His wing and tail lifts due to wing or tail plunge are over predicted by 5–10% relative to kernel function results but agreement is improved considerably when the number of spanwise boxes is increased (4% difference). In application of another doublet-lattice method, a smaller number of spanwise boxes gave better agreement indicating the oscillations possible in comparisons between methods.

Other comparisons were made by AFFDL for the Laschka-Schmid wing-tail. These were for $M = 0$ and $\omega s/V = 1.0$. Agreement among the Laschka-Schmid kernel function results, the Albano kernel function, and the two versions of the doublet-lattice results is shown in Table VIII to be excellent for all generalized force coefficients. The maximum deviation was noticed in the imaginary part of tail lift due to wing plunge where the value from the Albano kernel method was 16% high. However, the total vector would be far less affected because of the much larger real part. The results from the doublet-lattice method agree extremely well with both of the above kernel method results. The largest deviations are in the four tail pitch generalized force coefficients. Here, the doublet-lattice results were 5 to 6% higher than kernel method values.

3.2 The Mach Box Method for T-Tails and Cruciform Tails

The basic difference between this program[24] and earlier methods for surfaces with folded tips is that the source strength is allowed to have a $1/y$ singularity in the two rows of boxes adjacent to a line of intersection. The other difference is that the possible geometries have been extended to T-tails and V-tails. Because of the size and complexity of the computer program, these changes have not been completely checked out. The following results are not considered to be final and some problems may exist in this development.

One application has been to an aspect ratio 4 rectangular wing with folded tip at constant angle of attack, zero frequency and $M_\infty = \sqrt{2}$. Exact results are available for comparison from Rodemich[22]. Figure 11 gives the $C_{l\alpha}$ as a function of tip fold angle. Comparison can be made with the exact results of Rodemich and the results of Donato[22] using an earlier version of a Mach box program. The predicted value of $C_{l\alpha}$ is consistently high, although increasing the number of boxes decreases the error. Figure 11 also gives spanwise plots of the velocity potential at the trailing edge for tip fold angles of 30°, 60°, 90°. The 90° data can also be compared with that of Rodemich. The most apparent feature of these plots is the rapid change in potential near the fold line due to the introduction of the $1/y$ strength singularity. Calculations were also performed on the AGARD T-tails and cruciform tail, Figure 12. Figure 13 is a plot of a few of the generalized force coefficients for the T-tails compared with some similar results from the first order piston theory. The agreement shown is good for higher Mach numbers and gives some confidence in the order of magnitude of the Mach box results. Tables IX and X give all of the generalized force coefficients from the Mach box method and piston theory for $k = 0$ and 1.5 for the T-tail. Table XI gives the Mach box results for the cruciform AGARD tail.

4. CONCLUSIONS AND RECOMMENDATIONS

The opportunity to perform calculations for standard planforms, mode shapes, and flight conditions and to compare them with the results of other investigators has proved to be most valuable and provide stimulus to further research in the USA.

Generally, the kernel function and doublet-lattice methods agree well for a variety of conditions. However, some noticeable differences exist as discussed. More detailed investigation is required to explain all of these differences, but some are due to limits of multi lifting methods as discussed by investigators such as Stark, Landahl[34] and Laschka.

For consistent accuracy the doublet-lattice methods require a larger number of unknowns than the kernel function method, and so usually require greater computer expense. For some of the cases reported herein, a 15 x 3 kernel function analysis can be made in about half the time of an 81 box doublet-lattice analysis. Increasing the number of boxes from 81 to 144 more than doubles the computer running time. However, the lattice methods are quite new and may respond to numerical refinements and optimization.

Perhaps, a next logical step would be the comparison of theories with a standard set of experimental data.

ACKNOWLEDGEMENT

The authors gratefully extend thanks to Mr L.Huttsell, Mr T.Noll, and other members of the Vehicle Dynamics Division, US Air Force Flight Dynamics Laboratory for their contributions to this paper.

REFERENCES

1. Küssner, H. — *General Airfoil Theory.* Luftfahrtforschung, Bd.17, Lfg 11/12, December 10, 1940, NACA TM 979, 1941.

2. Watkins, C.E., et al. — *On the Kernel Function of the Integral Equation Relating the Lift and Downwash Distributions of Oscillating Finite Wings in Subsonic Flow.* NACA Report 1234, September 1953.

3. Watkins, C.E., et al. — *A Systematic Kernel Function Procedure for Determining Aerodynamic Forces on Oscillating or Steady Finite Wings at Subsonic Speeds.* NASA Technical Report R-48, 1959.

4. Rowe, W.S. — *Collocation Method for Calculating the Aerodynamic Pressure Distributions on a Lifting Surface Oscillating in Subsonic Compressible Flow.* Proceedings of the AIAA Symposium on Structural Dynamics and Aeroelasticity, Boston, Mass., USA, 1965.

5. Cunningham, A.M. — *A Rapid and Stable Subsonic Collocation Method for Solving Oscillatory Lifting Surface Problems by the Use of Quadrature Integration.* AIAA/ASME 11th Structures, Structural Dynamics and Materials Conference, Denver, Colorado, 22–24 April 1970.

6. Albano, E., Rodden, W.P. — *A Doublet-Lattice Method for Calculating Lift Distribution on Oscillating Surfaces in Subsonic Flows.* AIAA Journal, Vol.7, No.2, February 1969.

7. Berman, J.H., et al. — *Unsteady Aerodynamic Forces for General Wing/Control-Surface Configurations.* AFFDL-TR-67-117, May 1968.

8. Landahl, M. — *Pressure Loading Functions for Oscillating Wings with Control Surfaces.* AIAA Journal, Vol.6, No.2, February 1968.

9. Ashley, H., Rowe, W.S. — *On the Unsteady Aerodynamic Loading of Wings with Control Surfaces.* Dedication to Professor H.G.Küssner's Seventieth Birthday, May 1970.

10. Ashley, H. — *Linearized Time Dependent Loading of Intersecting Lifting Surfaces.* North American Aviation, Inc., Report SID-63-1020, 1963.

11. Ashley, H. — *Supersonic Airloads on Interfering Lifting Surfaces by Aerodynamic Influence Coefficient Theory.* The Boeing Company Report No.D2-22067, November 1962.

12. Ashley, H., et al. — *New Directions in Lifting Surface Theory.* AIAA Journal, Vol.3, January 1965.

13. Zartarian, G., Hsu, P.T — *Theoretical Studies on the Prediction of Unsteady Supersonic Airloads on Elastic Wings. Part I. Investigations on the Use of Oscillatory Supersonic Aerodynamic Influence Coefficients.* Wright Air Development Center Technical Report 56-97, Part I, December 1955.

14. Zartarian, G. — *Theoretical Studies on the Prediction of Unsteady Supersonic Airloads on Elastic Wings. Part II. Rules for Application of Oscillatory Supersonic Aerodynamic Influence Coefficients.* Wright Air Development Center Technical Report 56-97, Part II, February 1956.

15. Weatherill, W.H., Zartarian, G. — *Application of Methods for Analyzing the Flutter of Finite Wings in Supersonic Flow.* Wright Air Development Center Technical Report 58-459, December 1958.

16. Vivian, H.T., Andrew L.V. — *Unsteady Aerodynamics for Advanced Configurations. Part I. Application of the Subsonic Kernel Function to Nonplanar Surfaces.* Air Force Flight Dynamics Laboratory Report, FDL-TDR-64-152, Part I, May 1965.

17. Rodemich, E.R., Andrew, L.V. — *Unsteady Aerodynamics for Advanced Configurations. Part II. A Transonic Box Method for Planar Lifting Surfaces.* FDL-TDR-64-152, May 1965.

18. Moore, M.T., Andrew, L.V. — *Unsteady Aerodynamics for Advanced Configurations. Part IV. Application of the Supersonic Mach Box Method to Intersecting Planar Lifting Surfaces.* Air Force Flight Dynamics Laboratory Technical Documentary Report, FDL-TDR-64-152, Part IV, May 1965.

19. Andrew, L.V. — *Unsteady Aerodynamics for Advanced Configurations. Part VI. A Supersonic Mach Box Method Applied to T-Tails, V-Tails, and Top-Mounted Vertical Tails.* Air Force Flight Dynamics Laboratory Technical Documentary Report, FDL-TDR-64-152, Part VI, (to be issued).

20. Andrew, L.V., Stenton, T.E. — *Unsteady Aerodynamics for Advanced Configurations. Part VIII. Velocity Potentials in Non-Uniform Transonic Flow Over a Thin Wing.* FDL-TDR-64-152, August 1968.

21. Stenton, T.E., Andrew, L.V. — *Transonic Unsteady Aerodynamics for Planar Wings with Trailing Edge Control Surfaces.* AFFDL-TR-67-180, August 1968.

22. Donato, V.W. Huhn, C.R., Jr — *Supersonic Unsteady Aerodynamics for Wings with Trailing Edge Control Surfaces and Folded Tips.* Air Force Flight Dynamics Laboratory Technical Report, AFFDL-TR-68-30, August 1968.

23. Albano, E., et al. — *Subsonic Lifting Surface Theory Aerodynamics for Flutter Analysis of Interfering Wing/Horizontal Tail Configurations.* AFFDL-TR-70-59, March 1970.

24. Andrew, L.V. — *Unsteady Aerodynamics for Advanced Configurations. A Subsonic Kernel Function Method Applied to T-Tails, V-Tails and Tandem Surfaces.* US Air Force Flight Dynamics Laboratory Technical Report (to be published).

25. Kalman, T. et al. — *Subsonic Unsteady Aerodynamics for Wing-Fuselage and Wing-Pylon-Store Combinations.* AFFDL Report (to be published).

26. Laschka, B. — *The Potential and the Velocity Field for the Harmonically Oscillating Lifting Surface in Subsonic Streams.* ZAMM Vol.43, No.7/8, 1963.

27. Laschka, B., Schmid, H. — *Unsteady Aerodynamic Forces on Coplanar Lifting Surfaces in Subsonic Flow. Wing-Horizontal Tail Interference.* Vereinigte Flugtechnische Werke GmbH Entwicklungs-Abteilung, München, Germany, Report VFW M-72/66, December 1966.

28. Laschka, B. — *Interfering Lifting Surfaces in Subsonic Flow.* 29th AGARD Structures and Materials Panel Meeting, Istanbul, Turkey, 28 September – 8 October 1969.

29. Landahl, M.T. — *Kernel Function for Nonplanar Oscillating Surfaces in a Subsonic Flow.* AIAA Journal 5, May 1967.

30. Stark, V.J.E. — *Aerodynamic Forces on a Combination of a Wing and a Fin Oscillating in Subsonic Flow.* Svenska Aeroplane Aktiebolaget Report Saab TN 54, February 1964.

31. Kalman, T. et al. — *Application of the Doublet-Lattice Method to Nonplanar Configurations in Subsonic Flow.* AIAA Atmospheric Flight Mechanics Conference, University of Tennessee Space Institute, May 1970.

32. Balcerak, J.C. — *Flutter Tests of Variable Sweep Configurations.* US Flight Dynamics Laboratory Technical Report, AFFDL-TR-68-101, September 1968.

33. Mykytow, W.J. et al. — *Subsonic Flutter Characteristics of a Variable Sweep Wing and Horizontal Tail Combination.* Air Force Flight Dynamics Laboratory Technical Report, AFFDL-TR-69-59, (to be published).

34. Landahl, M.T., Stark, V.J.E. — *Numerical Lifting-Surface Theory – Problems and Progress.* AIAA Paper 68-72, AIAA 6th Aerospace Sciences Meeting, January 1968.

TABLE I

Generalized Force Coefficients for Isolated Surfaces, $M_\infty = 0.8$, $s\omega/V = 0.01$ and 1.5

			Q′		Q″	
sω/V	*Generalized Force Coefficient in*	*Due to Pressure in*	*Doublet Lattice*	*Kernel Function*	*Doublet Lattice*	*Kernel Function*
0.01	Wing bending	Wing bending	0.0	0.0	0.2047	0.1839
	Wing bending	Wing twist	0.2852	0.2606	0.3805	0.3803
	Wing twist	Wing bending	0.0	0.0	−0.0441	−0.0517
	Wing twist	Wing twist	−0.0731	−0.0874	0.1662	0.1727
	Tail roll	Tail roll	0.0	0.0	0.4024	0.3746
	Tail roll	Tail pitch	0.6874	0.6337	0.7173	0.6978
	Tail pitch	Tail roll	0.0	0.0	0.1770	0.1518
	Tail pitch	Tail pitch	0.2075	0.1862	0.5796	0.5612
1.5	Wing bending	Wing bending	−0.3418	−0.3480	0.2171	0.2074
	Wing bending	Wing twist	0.2115	0.2121	0.4025	0.4138
	Wing twist	Wing bending	−0.1883	−0.1351	−0.0417	−0.0504
	Wing twist	Wing twist	−0.1651	−0.2020	0.1617	0.1942
	Tail roll	Tail roll	−0.2960	−0.3161	0.4299	0.4214
	Tail roll	Tail pitch	0.5397	0.5321	0.7615	0.7718
	Tail pitch	Tail roll	−0.2763	−0.3115	0.1982	0.1826
	Tail pitch	Tail ptich	0.0193	−0.0446	0.6245	0.6443

TABLE II

Generalized Force Coefficients for Coplanar Surfaces, $M_\infty = 0.8$, $s\omega/V = 0.01$

		Q′		Q″	
Generalized Force Coefficient in	*Due to Pressure in*	*Doublet Lattice*	*Kernel Function*	*Doublet Lattice*	*Kernel Function*
Wing bending	Wing bending	0.0	0.0	0.2040	0.1764
Wing bending	Wing twist	0.2792	0.2463	0.3987	0.3912
Wing bending	Tail roll	0.0	0.0	0.0155	0.0153
Wing bending	Tail pitch	0.0342	0.0342	−0.0005	−0.0045
Wing twist	Wing bending	0.0	0.0	−0.0480	−0.0558
Wing twist	Wing twist	−0.0801	−0.0954	0.1657	0.1774
Wing twist	Tail roll	0.0	0.0	0.0074	0.0086
Wing twist	Tail pitch	0.0164	0.0193	0.0021	0.0002
Tail roll	Wing bending	0.0	0.0	−0.2602	−0.2362
Tail roll	Wing twist	−0.3753	−0.3471	0.0374	−0.0008
Tail roll	Tail roll	0.0	0.0	0.3947	0.3568
Tail roll	Tail pitch	0.6491	0.5928	0.7618	0.7394
Tail pitch	Wing bending	0.0	0.0	−0.1348	−0.1132
Tail pitch	Wing twist	−0.1685	−0.1409	−0.0065	−0.0304
Tail pitch	Tail roll	0.0	0.0	0.1707	0.1405
Tail pitch	Tail pitch	0.1895	0.1612	0.5851	0.5811

TABLE III

Generalized Force Coefficients for Coplanar Surfaces, $M_\infty = 0.8$, $s\omega/V = 1.5$

		Q′		Q″	
Generalized Force Coefficient in	*Due to Pressure in*	*Doublet Lattice*	*Kernel Function*	*Doublet Lattice*	*Kernel Function*
Wing bending	Wing bending	−0.3470	−0.3587	0.2330	0.2177
Wing bending	Wing twist	0.2274	0.2146	0.4145	0.4334
Wing bending	Tail roll	0.0190	0.0218	0.0093	0.0086
Wing bending	Tail pitch	0.0415	0.0401	−0.0175	−0.0244
Wing twist	Wing bending	−0.1277	−0.1440	−0.0345	−0.0450
Wing twist	Wing twist	−0.1603	−0.2054	0.1795	0.2073
Wing twist	Tail roll	0.0095	0.0132	0.0059	0.0064
Wing twist	Tail pitch	0.0245	0.0287	−0.0077	−0.0140
Tail roll	Wing bending	−0.4147	−0.3784	−0.1399	−0.1579
Tail roll	Wing twist	−0.5584	−0.5887	0.1448	0.1181
Tail roll	Tail roll	−0.3123	−0.3399	0.4466	0.4315
Tail roll	Tail pitch	0.5615	0.5505	0.7868	0.8097
Tail pitch	Wing bending	−0.1921	−0.1488	−0.1027	−0.1149
Tail pitch	Wing twist	−0.2754	−0.2737	0.0395	−0.0028
Tail pitch	Tail roll	−0.2832	−0.3315	0.2085	0.1876
Tail pitch	Tail pitch	0.0100	−0.0430	0.6287	0.6740

TABLE IV

Generalized Force Coefficients for $\Delta z = 0.6$, $M_\infty = 0.8$, $s\omega/V = 0.01$. Kernel Function Method

		Q′		Q″	
Generalized Force Coefficient in	*Due to Pressure in*	*Coplanar*	$\Delta z = 0.6$	*Coplanar*	$\Delta z = 0.6$
Wing bending	Wing bending	0.0	0.0	0.1764	0.1842
Wing bending	Wing twist	0.2463	0.2611	0.3912	0.3804
Wing bending	Tail roll	0.0	0.0	0.0153	−0.0019
Wing bending	Tail pitch	0.0342	−0.0049	−0.0045	−0.0009
Wing twist	Wing bending	0.0	0.0	−0.0558	−0.0515
Wing twist	Wing twist	−0.0954	−0.0871	0.1774	0.1726
Wing twist	Tail roll	0.0	0.0	0.0086	−0.0014
Wing twist	Tail pitch	0.0193	−0.0033	0.0002	0.0005
Tail roll	Wing bending	0.0	0.0	−0.2362	−0.0395
Tail roll	Wing twist	−0.3471	−0.0619	−0.0008	0.0044
Tail roll	Tail roll	0.0	0.0	0.3568	0.3749
Tail roll	Tail pitch	0.5928	0.6345	0.7394	0.6975
Tail pitch	Wing bending	0.0	0.0	−0.1132	−0.0138
Tail pitch	Wing twist	−0.1409	−0.0206	−0.0304	0.0025
Tail pitch	Tail roll	0.0	0.0	0.1405	0.1519
Tail pitch	Tail pitch	0.1612	0.1866	0.5811	0.5611

TABLE V

Generalized Force Coefficients for $\Delta z = 0.6$, $M_\infty = 0.8$, $s\omega/V = 1.5$. Kernel Function Method

		Q′		Q″	
Generalized Force Coefficient in	*Due to Pressure in*	*Coplanar*	$\Delta z = 0.6$	*Coplanar*	$\Delta z = 0.6$
Wing bending	Wing bending	−0.3587	−0.3478	0.2177	0.2083
Wing bending	Wing twist	0.2146	0.2147	0.4334	0.4145
Wing bending	Tail roll	0.0218	−0.0026	0.0086	−0.0052
Wing bending	Tail pitch	0.0401	−0.0156	−0.0244	−0.0012
Wing twist	Wing bending	−0.1440	−0.1360	−0.0450	−0.0507
Wing twist	Wing twist	−0.2054	−0.2035	0.2073	0.1952
Wing twist	Tail roll	0.0132	−0.0008	0.0064	−0.0031
Wing twist	Tail pitch	0.0287	−0.0087	−0.0140	−0.0016
Tail roll	Wing bending	−0.3784	−0.0431	−0.1579	−0.0137
Tail roll	Wing twist	−0.5887	−0.0615	0.1181	0.0246
Tail roll	Tail roll	−0.3399	−0.3156	0.4315	0.4215
Tail roll	Tail pitch	0.5505	0.5328	0.8097	0.7713
Tail pitch	Wing bending	−0.1488	−0.0192	−0.1149	−0.0049
Tail pitch	Wing twist	−0.2737	−0.0232	−0.0028	0.0108
Tail pitch	Tail roll	−0.3315	−0.3115	0.1876	0.1825
Tail pitch	Tail pitch	−0.0430	−0.0452	0.6740	0.6442

TABLE VI

Generalized Force Coefficients for 30°, 0°, −30° Dihedral,
$M_\infty = 0.8$, $\Delta z = 0.6$, $s\omega/V = 0.01$

		Q′			Q″		
Generalized Force Coefficient in	*Due to Pressure in*	30°	0°	−30°	30°	0°	−30°
Wing bending	Wing bending	0.0	0.0	0.0	0.1843	0.1842	0.1832
Wing bending	Wing twist	0.2613	0.2611	0.2594	0.3801	0.3804	0.3820
Wing bending	Tail roll	0.0	0.0	0.0	−0.0035	−0.0019	0.0051
Wing bending	Tail pitch	−0.0089	−0.0049	0.0108	0.0015	−0.0009	−0.0028
Wing twist	Wing bending	0.0	0.0	0.0	−0.0515	−0.0515	−0.0520
Wing twist	Wing twist	−0.0870	−0.0871	−0.0880	0.1726	0.1726	0.1732
Wing twist	Tail roll	0.0	0.0	0.0	−0.0018	−0.0014	0.0024
Wing twist	Tail pitch	−0.0044	−0.0033	0.0048	0.0	0.0005	0.0005
Tail roll	Wing bending	0.0	0.0	0.0	−0.0248	−0.0395	−0.0719
Tail roll	Wing twist	−0.0386	−0.0619	−0.1193	0.0019	0.0044	0.0336
Tail roll	Tail roll	0.0	0.0	0.0	0.3684	0.3749	0.3670
Tail roll	Tail pitch	0.6207	0.6345	0.6172	0.6747	0.6975	0.6806
Tail pitch	Wing bending	0.0	0.0	0.0	−0.0059	−0.0138	−0.0386
Tail pitch	Wing bending	−0.0088	−0.0206	−0.0610	0.0016	0.0025	0.0123
Tail pitch	Tail roll	0.0	0.0	0.0	0.1484	0.1519	0.1478
Tail pitch	Tail pitch	0.1809	0.1866	0.1791	0.5468	0.5611	0.5498

TABLE VII

Generalized Force Coefficients for 30°, 0°, −30° Dihedral,
$M_\infty = 0.8$, $\Delta z = 0.6$, $s\omega/V = 1.5$

		Q′			Q″		
Generalized Force Coefficient in	*Due to Pressure in*	30°	0°	−30°	30°	0°	−30°
Wing bending	Wing bending	−0.3478	−0.3478	−0.3479	0.2083	0.2083	0.2091
Wing bending	Wing twist	0.2146	0.2147	0.2158	0.4144	0.4145	0.4153
Wing bending	Tail roll	−0.0078	−0.0026	0.0096	−0.0018	−0.0052	0.0
Wing bending	Tail pitch	−0.0129	−0.0156	0.0083	0.0098	−0.0012	−0.0132
Wing twist	Wing bending	−0.1360	−0.1360	−0.1361	−0.0507	−0.0507	−0.0502
Wing twist	Wing twist	−0.2035	−0.2035	−0.2029	0.1951	0.1952	0.1958
Wing twist	Tail roll	−0.0043	−0.0008	0.0058	−0.0016	−0.0031	0.0006
Wing twist	Tail pitch	−0.0094	−0.0087	0.0074	0.0049	−0.0016	−0.0073
Tail roll	Wing bending	−0.0149	−0.0431	−0.1233	−0.0097	−0.0137	−0.0151
Tail roll	Wing twist	−0.0320	−0.0615	−0.1457	0.0026	0.0247	0.0791
Tail roll	Tail roll	−0.3084	−0.3156	−0.3075	0.4044	0.4215	0.4057
Tail roll	Tail pitch	0.5027	0.5328	0.5080	0.7386	0.7713	0.7386
Tail pitch	Wing bending	−0.0034	−0.0192	−0.0672	0.0007	−0.0049	−0.0161
Tail pitch	Wing twist	−0.0011	−0.0232	−0.0898	0.0024	0.0108	0.0366
Tail pitch	Tail roll	−0.2983	−0.3115	−0.2978	0.1743	0.1825	0.1752
Tail pitch	Tail pitch	−0.0427	−0.0452	−0.0393	0.6158	0.6442	0.6160

TABLE VIII

Generalized Force Coefficients for Laschka-Schmid Wing Tail, M = 0 and $\omega s/V = 1.0$

Generalized Force Coefficient in	*Due to Pressure in*	*Kernel Function*				*Doublet Lattice*			
		Laschka-Schmid		*Albano*		*Albano-Rodden*		*Giesing-Kalman-Rodden*	
		Real	*Imag.*	*Real*	*Imag.*	*Real*	*Imag.*	*Real*	*Imag.*
Wing plunge	Wing plunge	−0.687	2.572	−0.688	2.577	−0.664	2.621	−0.638	2.603
Wing plunge	Tail plunge	0.011	0.059	0.016	0.057	0.014	0.061	0.014	0.061
Wing plunge	Wing pitch	2.078	3.344	2.082	3.349	2.122	3.396	2.116	3.359
Wing plunge	Tail pitch	0.102	0.032	0.102	0.025	0.107	0.034	0.106	0.033
Tail plunge	Wing plunge	−1.978	−0.525	−1.965	−0.549	−2.005	−0.552	−2.007	−0.566
Tail plunge	Tail plunge	−0.280	1.777	−0.280	1.784	−0.262	1.851	−0.262	1.853
Tail plunge	Wing pitch	−2.355	1.574	−2.366	1.537	−2.425	1.558	−2.439	1.553
Tail plunge	Tail pitch	2.475	2.255	2.484	2.259	2.591	2.325	2.592	2.326
Wing pitch	Wing plunge	−0.582	1.605	−0.582	1.608	−0.550	1.679	−0.539	1.670
Wing pitch	Tail plunge	0.007	0.046	0.010	0.045	0.009	0.047	0.009	0.047
Wing pitch	Wing pitch	1.127	2.506	1.129	2.509	1.215	2.551	1.211	2.535
Wing pitch	Tail pitch	0.078	0.029	0.078	0.024	0.081	0.029	0.081	0.029
Tail pitch	Wing plunge	−1.252	−0.313	−1.244	−0.329	−1.312	−0.331	−1.314	−0.340
Tail pitch	Tail plunge	−0.238	1.113	−0.238	1.118	−0.220	1.198	−0.221	1.199
Tail pitch	Wing pitch	−1.505	0.987	−1.513	0.963	−1.588	1.022	−1.598	1.021
Tail pitch	Tail pitch	1.480	1.684	1.486	1.687	1.617	1.749	1.618	1.751

TABLE IX

Generalized Aerodynamic Force Coefficients for the AGARD T-tail with Root Reflection Plane

			M = 1.2		M = 1.6	
sω/V	*Generalized Force Coefficient in*	*Due to Pressure in*	Q′	Q″	Q′	Q″
0	Stabilizer rock	Fin twist	0.5611	—	0.5621	—
	Fin bending	Fin twist	2.7991 (1) (1.8317) (2)	—	2.7068 (1.3738)	—
	Fin twist	Fin twist	0.4762 (0.3577)	—	0.3511 (0.2684)	—
1.5	Stabilizer rock	Stabilizer rock	−0.1074	0.6734 (1.0879)	0.0350	0.6700 (0.8160)
	Fin bending	Stabilizer rock	−0.2169	1.6167 (2.6107)	0.1251	1.6239 (1.9582)
	Fin twist	Stabilizer rock	0.0258	0.0008	0.0211	0.0074
	Stabilizer rock	Fin bending	−0.1562	1.7134 (2.6107)	0.4630	1.6933 (1.9582)
	Fin bending	Fin bending	−0.2820	4.4688 (7.6939)	1.3389	4.7124 (5.7705)
	Fin twist	Fin bending	0.0192	0.0534 (0.2366)	0.0664	0.1324 (0.1775)
	Stabilizer rock	Fin twist	0.3192	−0.0601	0.1392	−0.2333
	Fin bending	Fin twist	1.6081 (1.8317)	0.0563 (0.4731)	1.4164 (1.3738)	−0.4249 (0.3549)
	Fin twist	Fin twist	0.2122 (0.3577)	0.2028 (0.1889)	0.2823 (0.2684)	0.1817 (0.1417)

TABLE X

Generalized Aerodynamic Force Coefficients for the AGARD T-tail with Root Reflection Plane

			M = 2.0		M = 3.0	
sω/V	*Generalized Force Coefficient in*	*Due to Pressure in*	Q′	Q″	Q′	Q″
0	Stabilizer rock	Fin twist	0.3520	—	0.0765	—
	Fin bending	Fin twist	1.8227 (1) (1.0990) (2)	—	0.8540 (0.7327)	—
	Fin twist	Fin twist	0.2673 (0.2146)	—	0.1609 (0.1431)	—
1.5	Stabilizer rock	Stabilizer rock	0.0707	0.5531 (0.6527)	0.0190	0.4130 (0.4351)
	Fin bending	Stabilizer rock	0.1897	1.3359 (1.5663)	0.0527	0.9914 (1.0444)
	Fin twist	Stabilizer rock	0.0098	0.0040	0.0035	0.0014
	Stabilizer rock	Fin bending	0.3928	1.3078 (1.5663)	0.1161	0.9969 (1.0444)
	Fin bending	Fin bending	1.1030	3.6539 (4.6164)	0.4038	2.7904 (3.0776)
	Fin twist	Fin bending	0.0468	0.0937 (0.1420)	0.0475	0.0774 (0.0947)
	Stabilizer rock	Fin twist	−0.0681	−0.0743	−0.0031	−0.0223
	Fin bending	Fin twist	0.6240 (1.0990)	−0.0759 (0.2839)	0.5521 (0.7327)	0.0060 (0.1892)
	Fin twist	Fin twist	0.1788 (0.2146)	0.1407 (0.1134)	0.1248 (0.1431)	0.0854 (0.0755)

(1) Mach box method
(2) Piston theory

TABLE XI

Generalized Aerodynamic Force Coefficients for the AGARD Cruciform Tail with Root Reflection Plane

			M = 1.2		M = 1.6	
$s\omega/V$	*Generalized Force Coefficient in*	*Due to Pressure in*	Q′	Q″	Q′	Q″
0	Stabilizer rock	Fin twist	0.0334	—	−0.0478	—
	Fin bending	Fin twist	0.7425	—	0.7166	—
	Fin twist	Fin twist	0.1330	—	0.1200	—
1.5	Stabilizer rock	Stabilizer rock	−0.0995	0.7037	0.0468	0.6861
	Fin bending	Stabilizer rock	−0.2027	0.8000	−0.0212	0.7996
	Fin twist	Stabilizer rock	−0.0108	−0.0146	−0.0175	−0.0057
	Stabilizer rock	Fin bending	−0.3160	0.7435	−0.0969	0.8143
	Fin bending	Fin bending	−0.8264	1.2677	−0.5200	1.4796
	Fin twist	Fin bending	−0.0983	−0.0079	−0.1204	0.0265
	Stabilizer rock	Fin twist	−0.0595	0.0571	0.0360	0.0296
	Fin bending	Fin twist	0.5511	0.3776	0.8623	0.3133
	Fin twist	Fin twist	0.0618	0.1504	0.1303	0.1801

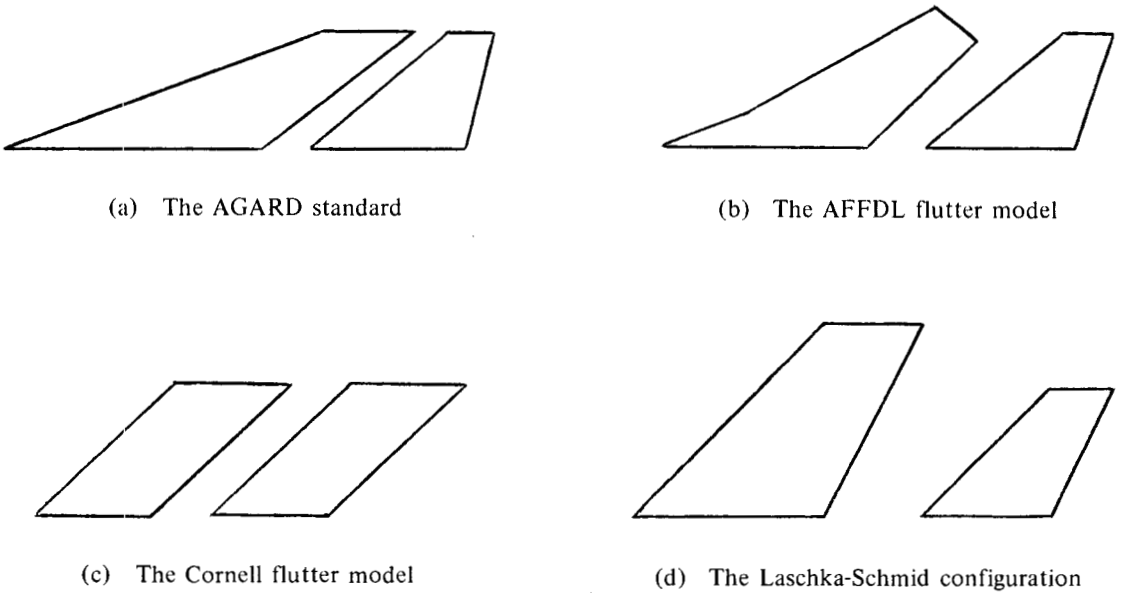

(a) The AGARD standard

(b) The AFFDL flutter model

(c) The Cornell flutter model

(d) The Laschka-Schmid configuration

Fig.1 Configurations used for subsonic calculations

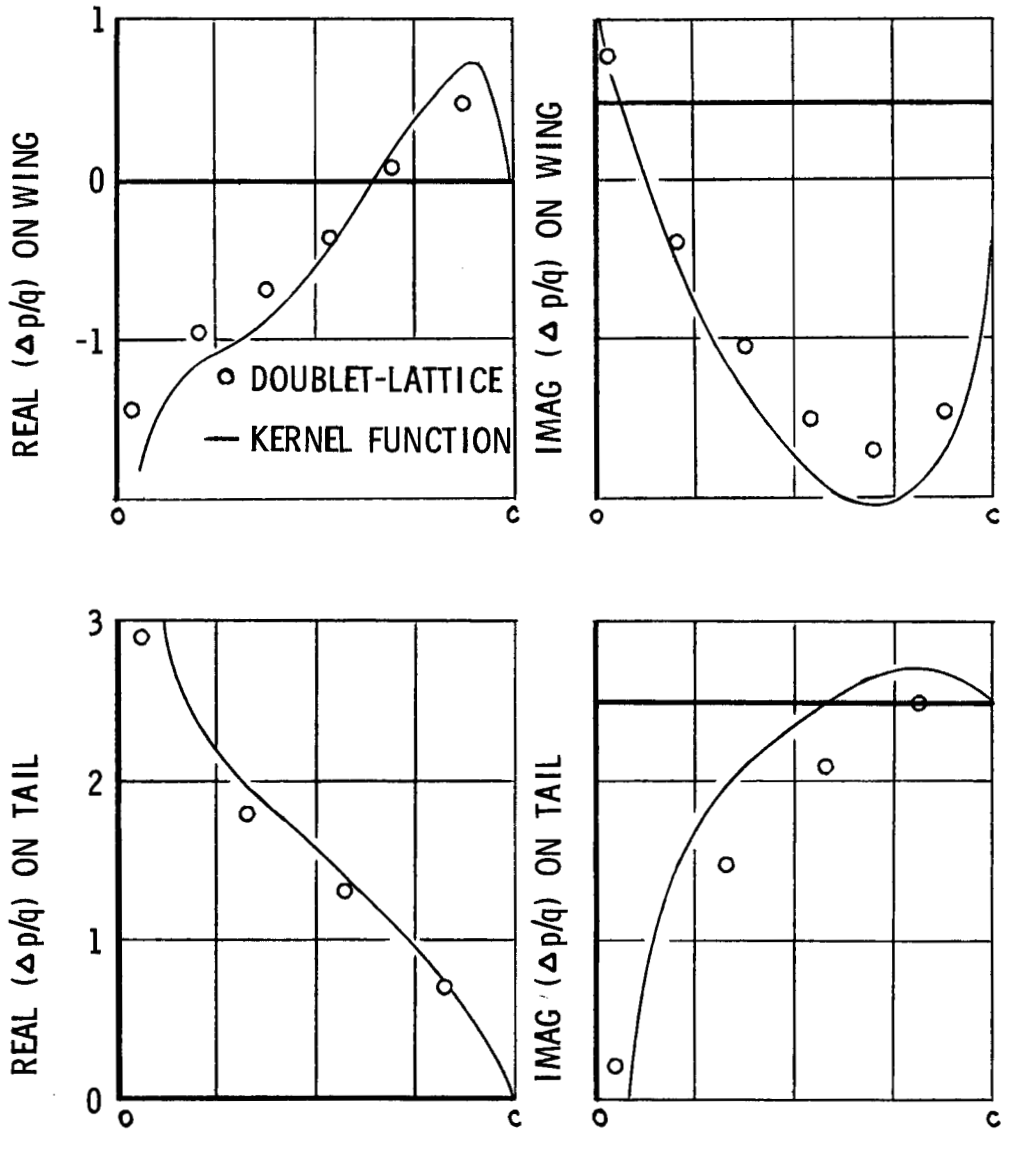

Fig.2 Chordwise distribution of $\Delta p/q$ due to wing twist, 56% semispan, $M_\infty = 0.8$, $s\omega/V = 1.5$

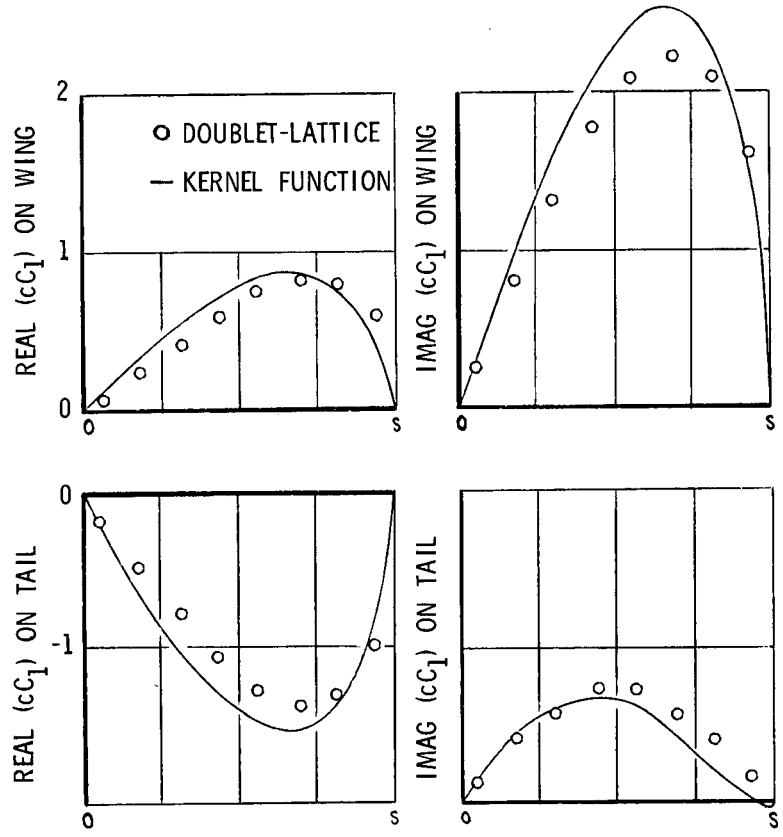

Fig.3 Spanwise distribution of $cC_l(y)$ due to wing twist, $M_\infty = 0.8$, $s\omega/V = 1.5$

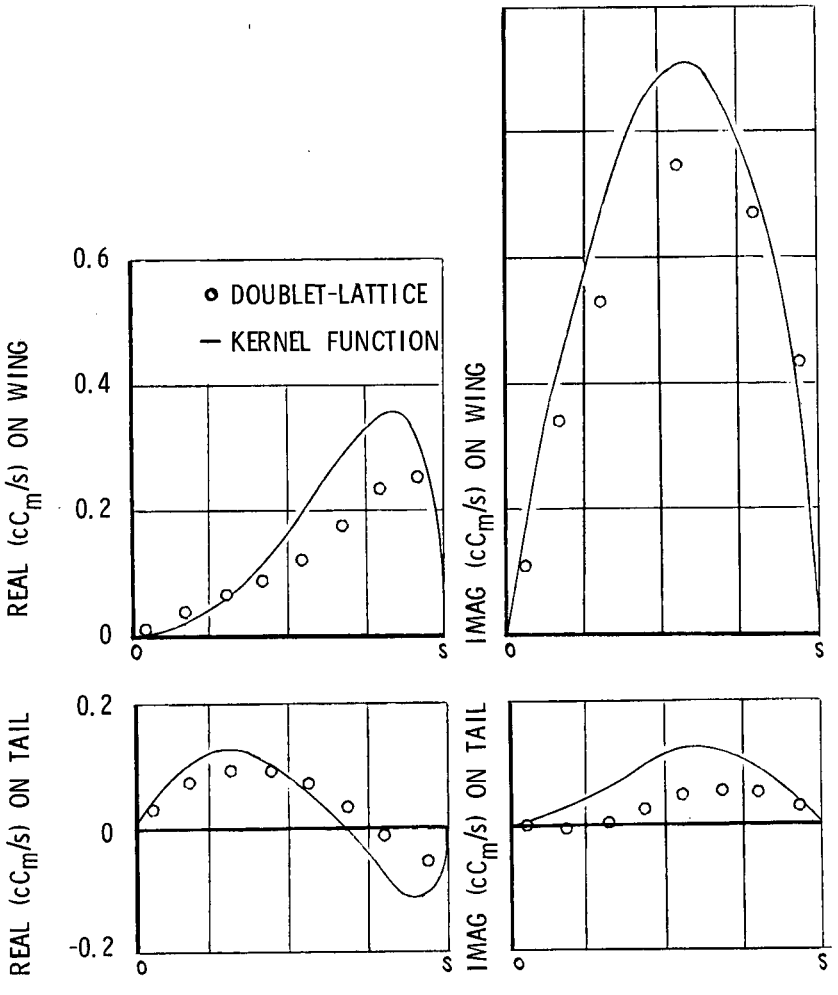

Fig.4 Spanwise distribution of cC_m/s due to wing twist, $M_\infty = 0.8$, $s\omega/V = 1.5$

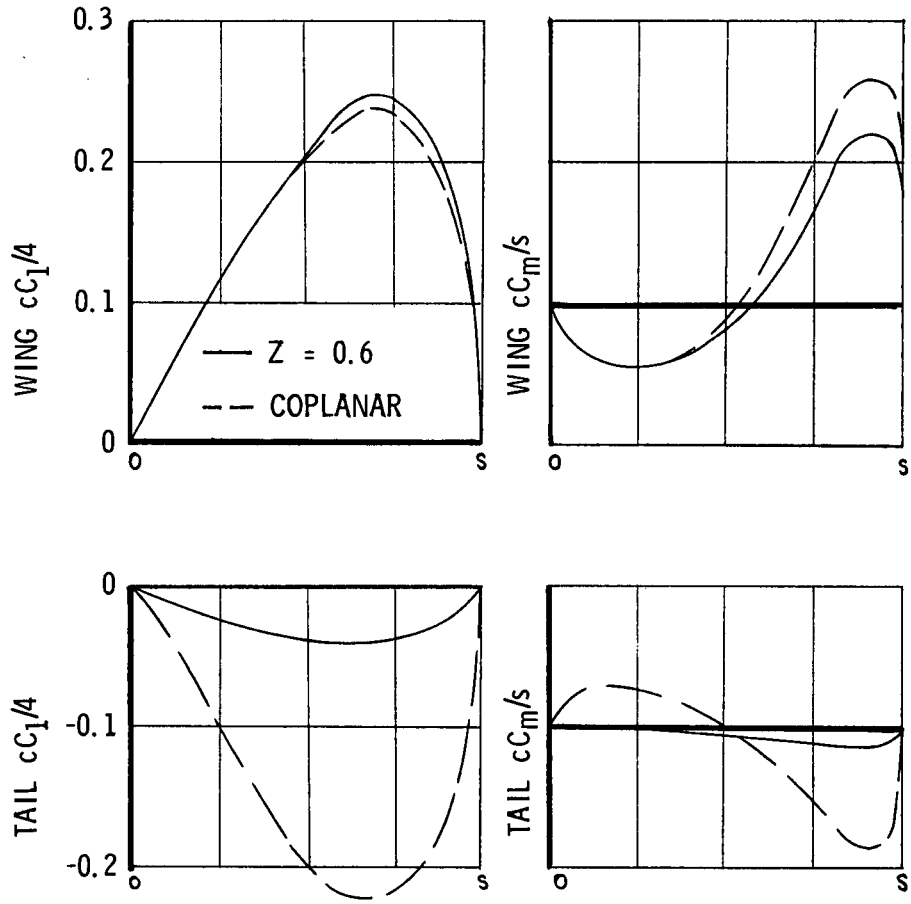

Fig.5 Spanwise distribution of $cC_l/4$ and cC_m/s due to wing twist with vertical separation, $M_\infty = 0.8$, $s\omega/V = 0.01$

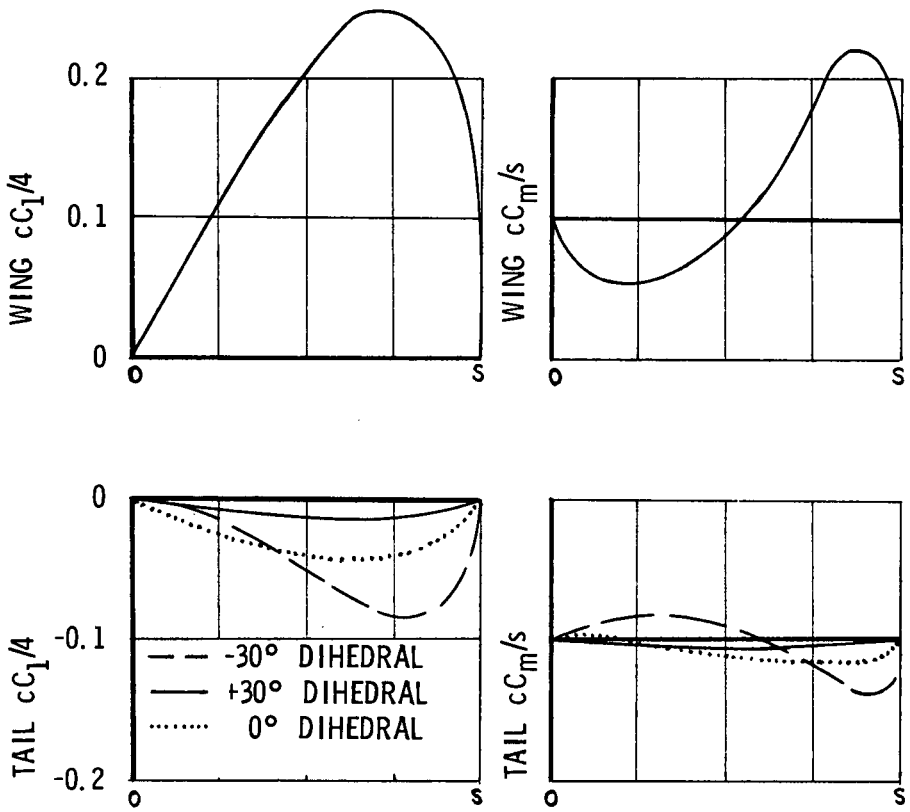

Fig.6 Spanwise distribution of $cC_l/4$ and cC_m/s due to wing twist with dihedral and vertical separation, $M_\infty = 0.8$, $s\omega/V = 0.01$

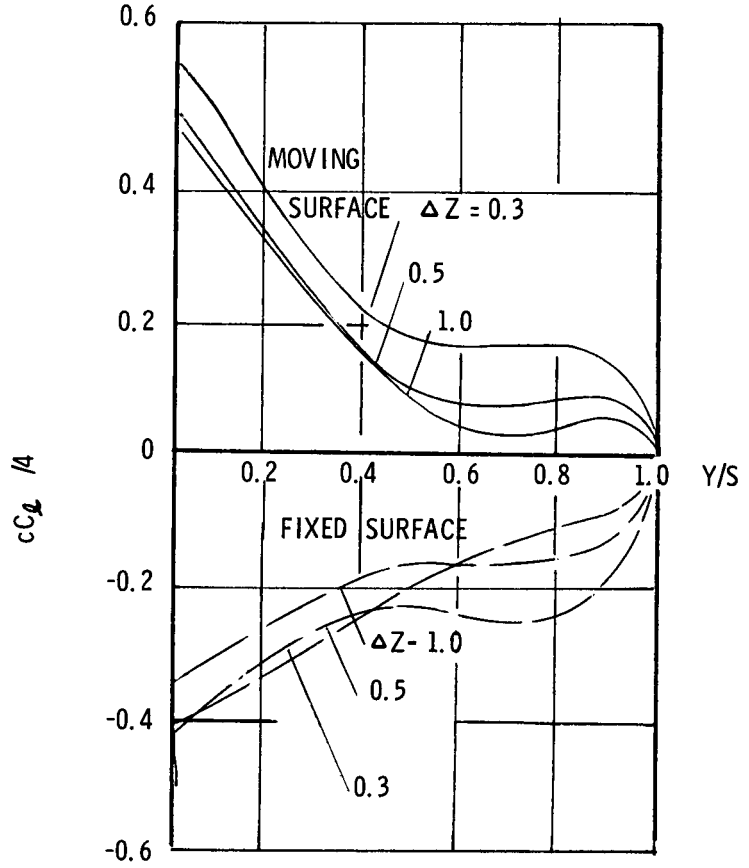

Fig.7 Real lift coefficient due to pitch of one surface of biplane, M = 0.8, sω/V = 1.0

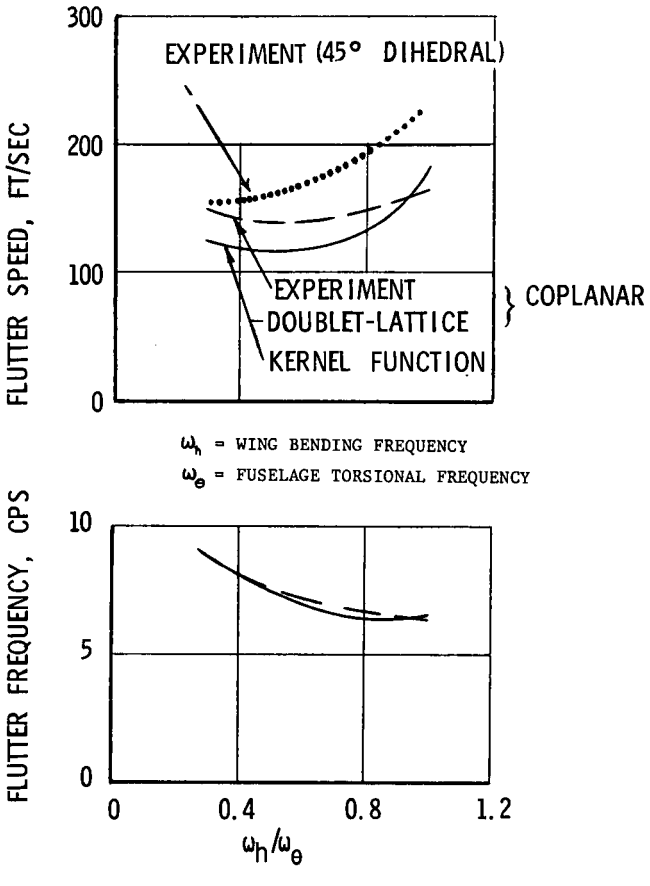

Fig.8 Flutter speed and frequency versus ω_h/ω_θ for the AFFDL flutter model, 60° sweep, Δx = 0.25 ft

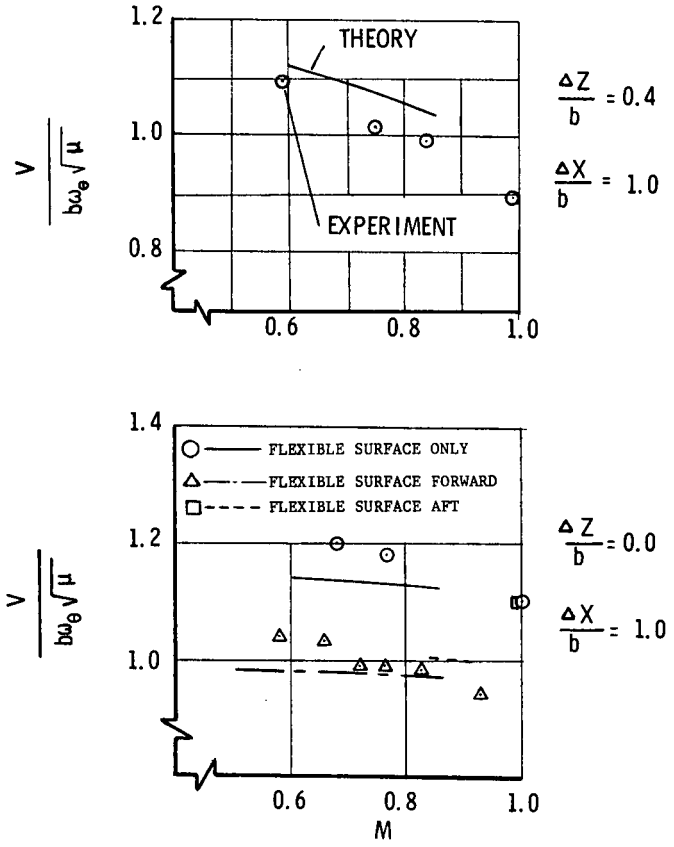

Fig.9 The Cornell transonic wing tail flutter model. Experimental and kernel function results

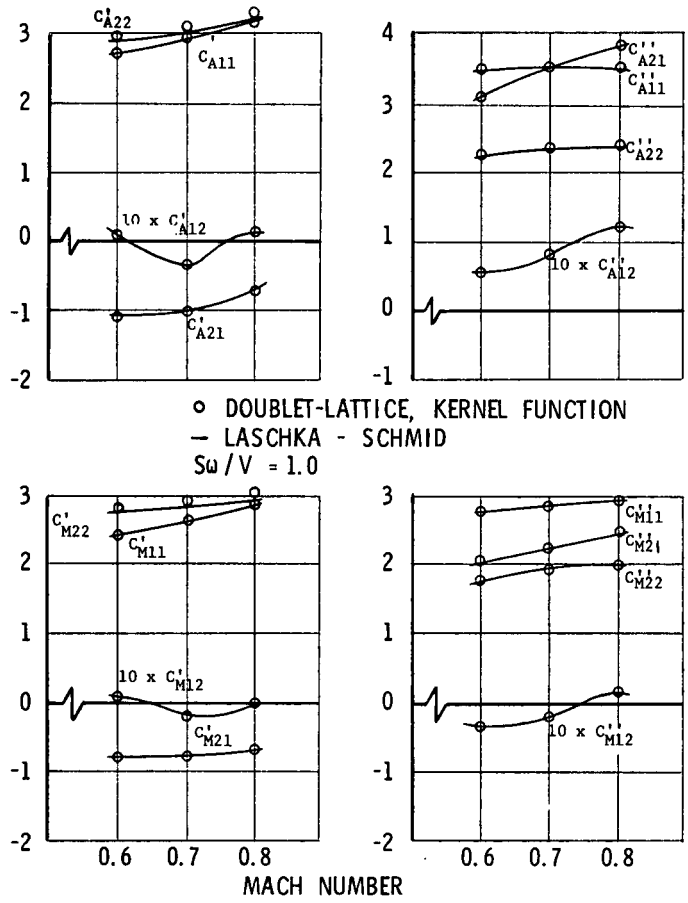

Fig.10 Lift and moment coefficients due to wing or tail pitch

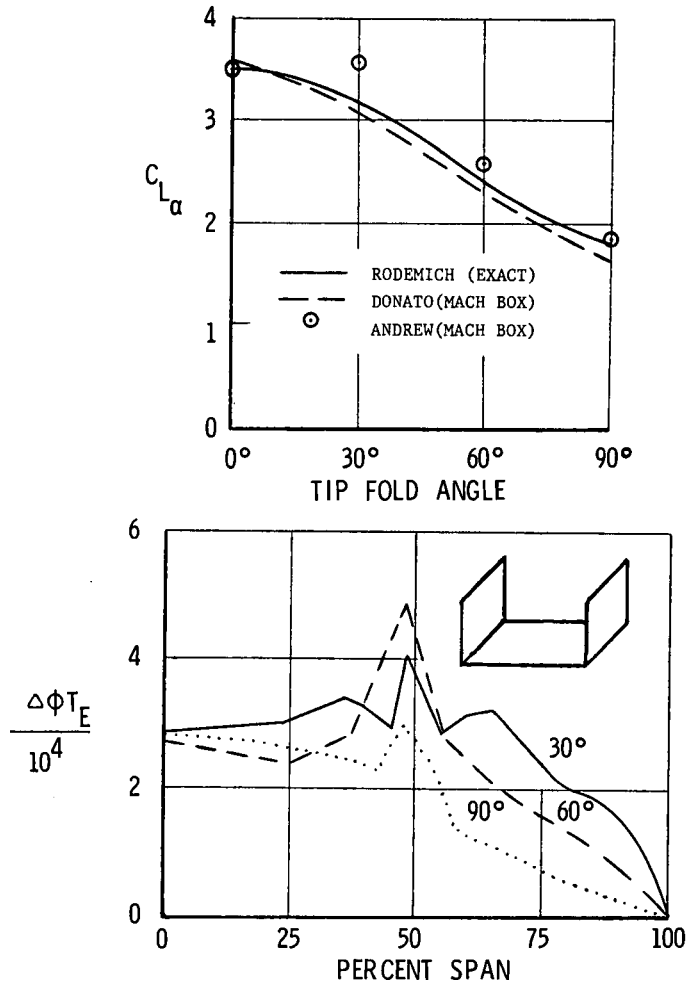

Fig.11 $C_{L\alpha}$ and $\Delta\phi_{TE}$ for an aspect ratio 4 rectangle with folded tip

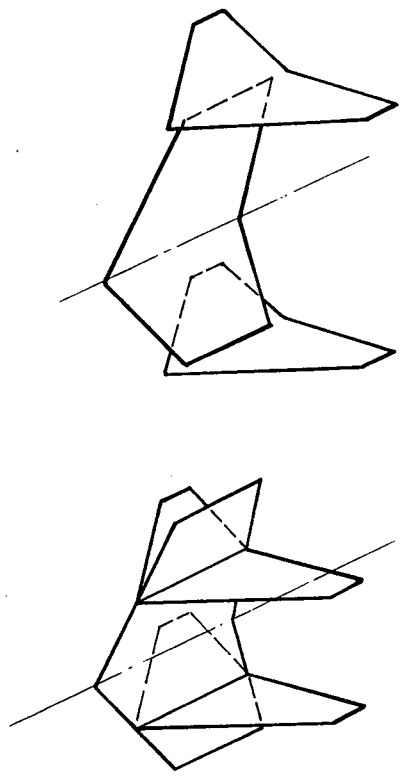

Fig.12 The AGARD T-tail and cruciform tail

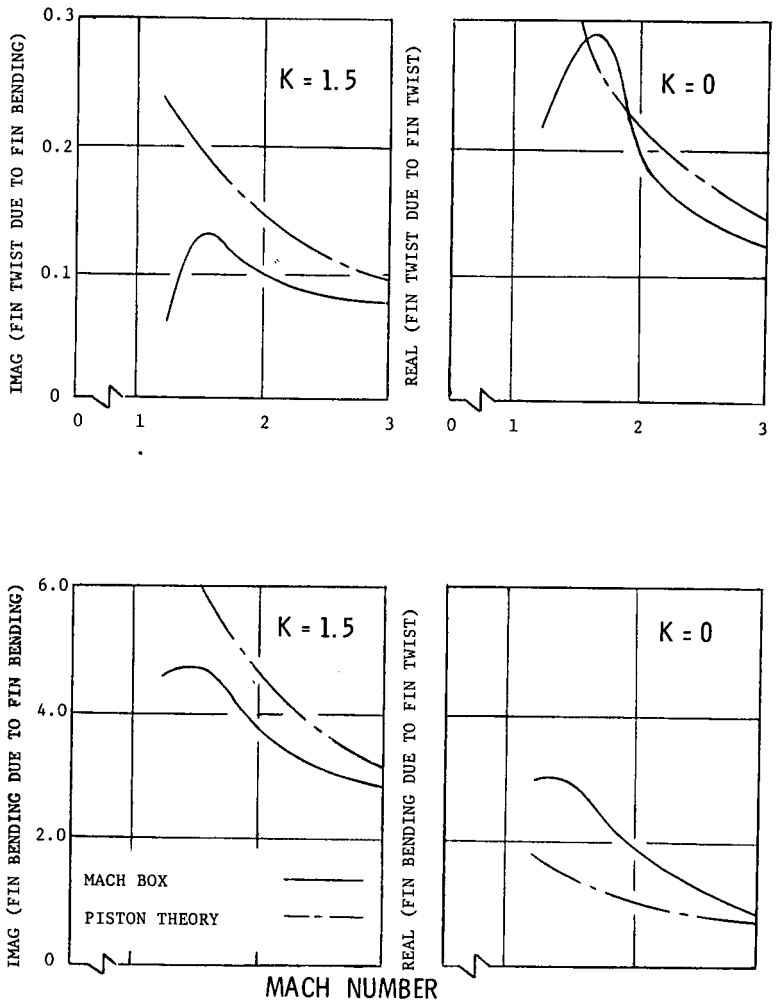

Fig. 13 Generalized aerodynamic forces on the AGARD T-tail with root reflection plane